Collective conflict resolution in groups on the move

Itai Pinkoviezky,[1] Iain D. Couzin,[2] and Nir S. Gov[3]
[1]*Departments of Physics and Biology, Emory University, Atlanta, Georgia 30322, USA*
[2]*Department of Collective Behaviour, Max Planck Institute for Ornithology, 78457 Konstanz, Germany and Department of Biology, University of Konstanz, 78457 Konstanz, Germany*
[3]*Department of Chemical Physics, Weizmann Institute of Science, Rehovot 7610001, Israel*

(Received 14 September 2017; published 12 March 2018)

Collective decision-making regarding direction of travel is observed during natural motion of animal and cellular groups. This phenomenon is exemplified, in the simplest case, by a group that contains two informed subgroups that hold conflicting preferred directions of motion. Under such circumstances, simulations, subsequently supported by experimental data with birds and primates, have demonstrated that the resulting motion is either towards a compromise direction or towards one of the preferred targets (even when the two subgroups are equal in size). However, the nature of this transition is not well understood. We present a theoretical study that combines simulations and a spin model for mobile animal groups, the latter providing an equilibrium representation, and exact solution in the thermodynamic limit. This allows us to identify the nature of this transition at a critical angular difference between the two preferred directions: in both flocking and spin models the transition coincides with the change in the group dynamics from Brownian to persistent collective motion. The groups undergo this transition as the number of uninformed individuals (those in the group that do not exhibit a directional preference) increases, which acts as an inverse of the temperature (noise) of the spin model. When the two informed subgroups are not equal in size, there is a tendency for the group to reach the target preferred by the larger subgroup. We find that the spin model captures effectively the essence of the collective decision-making transition and allows us to reveal a noise-dependent trade-off between the decision-making speed and the ability to achieve majority (democratic) consensus.

DOI: 10.1103/PhysRevE.97.032304

I. INTRODUCTION

Consider a group of animals on the move, such as a flock of birds, a school of fish, or a troop of baboons. The mechanisms describing the coherent motion and collective decision-making capabilities of such animal groups is a subject of great current interest for both biologists and physicists [1]. In many cases, organisms differ with respect to their knowledge or preferences within groups regarding where to go (such as with respect to foraging areas or of a migration route). To avoid losing the benefits of group living [2–5], many species maintain cohesion, with consensus being achieved via local interactions among group members [6,7].

When individuals differ with respect to their preferred directions of motion, there is an inherent conflict within the group. The simplest and most general example for such a conflict is when there are two informed subgroups, where the conflict is measured by the angular difference θ between the two preferred directions and the number of individuals in each subgroup. It was found in simulations of animal groups that when this angular difference is larger than a critical value θ_c the group switches, spontaneously, from compromise to a consensus decision to move in the direction of one or the other of the preferred directions [8]. Experimental observations in a wild troop of baboons [6] and pairs of pigeons [9] have demonstrated the existence of this transition from compromise to decision as a function of the angular conflict, but the nature of this transition is still not understood. There have been several attempts to explore the nature of this transition using simplified models [10,11]. However, these models did not replicate the consensus nature of the transition [10] or did not consider the motion of groups [11] and thus we lack an analytically tractable model of consensus decision-making in groups on the move.

Thus it is not clear which properties may influence the accuracy with which the collective decision is made to follow the majority-preferred direction or how properties such as noise influence decision-making dynamics. It has been shown theoretically [12] that following the majority, i.e., as in democracy, is often favorable since a majority is likely to have more reliable information and democratic consensus reduces compromise costs by preventing extreme decisions. However, with the exception of humans, animals that live in groups do not have the cognitive abilities to count a large number of votes [13,14]. Reference [15] studied the effect of informed subgroups of different sizes and strengths of preference as well as the role of the proportion of unbiased (or uninformed) individuals within the group on the consensus decision-making. However, how collective decision-making regarding directional preference emerges as a function of the system's parameters is lacking. Similarly, the conditions that optimize certain group properties, such as the capacity to select a majority-preferred direction, are not understood.

In order to address these deficiencies and to understand more clearly the process by which collectives make decisions, we present here a theoretical study that begins with a comprehensive numerical study of a spatial model of mobile animal groups moving in two-dimensional (2D) space. We then propose a simple, analytically tractable, spin model (first in

one dimension and then extended to two dimensions) to allow for better understanding of the collective conflict resolution phenomenology. Unlike previous spin models, we explicitly account for the group motion. In this model each informed individual can exert a social force on the group towards its preferred direction, but may not exert this force. This behavior allows us to treat the behavior of each informed individual as a spin degree of freedom, which makes the model Ising-like. For simplicity and tractability, it is assumed that individuals (spins) interact with all the other members of the group, which makes this model fully connected, nonspatial, and, by definition, cohesive. The group moves in space according to the sum of all exerted social forces. As in Ising models, the spin flips (individual decisions) are governed by the interplay between the interactions and noise (temperature). We solve the spin model using the mean-field method and compare it to the full spatial simulation of animal groups [8]. We find that there exists a trade-off between the accuracy, with respect to selecting correctly the majority-preferred direction, and the time traveled to a target location. We show that we can recover this finding in the fully spatial model of animal groups [8]. Since flocking models are essentially models of active matter [16], our model allows us to explore how much of the phenomenology is due to the active component and what can be explained within equilibrium theory.

II. DECISION TRANSITION IN A SPATIAL FLOCK MODEL

We begin by studying the decision transition in a well-established spatial model of collective motion in animal groups (which we call from now on the flock model) [8]. In Fig. 1(a) we show an illustration of the model, where the two informed subgroups are mixed with unbiased, or uninformed, individuals. The basis of this model is that each individual tries to move in the direction of motion of its local neighbors, similar to the well-known Vicsek model [17], with the addition of an attractive tendency that allows groups to remain cohesive. Note that the alignment is not an essential feature of the spatial

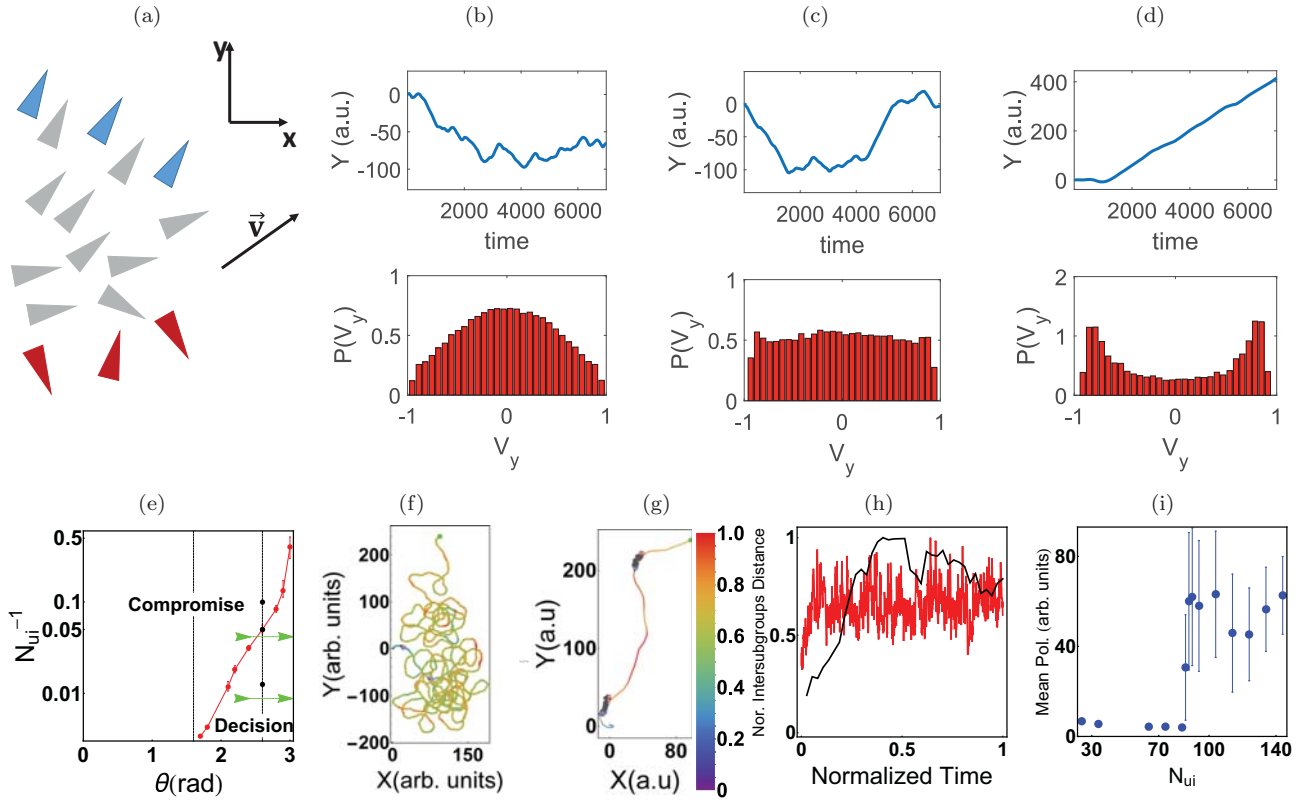

FIG. 1. (a) Illustration of the flock model. Gray agents represent the uninformed members, while the two informed subgroups are denoted by blue (subgroup 1) and red (subgroup 2) members. The depicted group tends to go in the direction of subgroup 1. Note that two members of the losing subgroup 2 are not oriented towards their preferred direction. (b)–(d) The trajectory of the Y coordinate (top) and the probability distribution of V_y (bottom) for angular difference $\theta = 2.6$ rad and (b) $N_{ui} = 10$, (c) $N_{ui} = 20$, and (d) $N_{ui} = 80$. (e) Phase diagram for the flock model as a function of the number of uninformed individuals N_{ui} and the angular conflict θ (the targets are at infinity). Results are obtained from simulations of a flock with two subgroups of size $N_1 = N_2 = 5$ and $\omega = 0.3$ [Eq. (A3)]. The angular difference of $\pi/2$ is denoted by a vertical dashed line. We also denote the angular difference of (b)–(d) by points corresponding to the different figures. Dashed green lines correspond to the trajectories of (f) and (g). (f) and (g) Examples of trajectories towards targets at finite distances, with normalized average distance between subgroups color coded along them, for (f) $N_{ui} = 24$ and (g) $N_{ui} = 114$. Clouds of points are snapshots of the group along the trajectory with the color code of (a). The targets (green points) are at $(x, y) = (100, \pm 250)$ relative to the flock initial location. (h) Normalized average distance between members in different subgroups against normalized time for $N_{ui} = 24$ (red) and $N_{ui} = 114$ (black). (i) Mean distance between the individuals in the two informed subgroups, from simulations of flocks containing a different number of uninformed individuals N_{ui} [as in (f)–(h)]. The mean distance is normalized by the number of uninformed individuals.

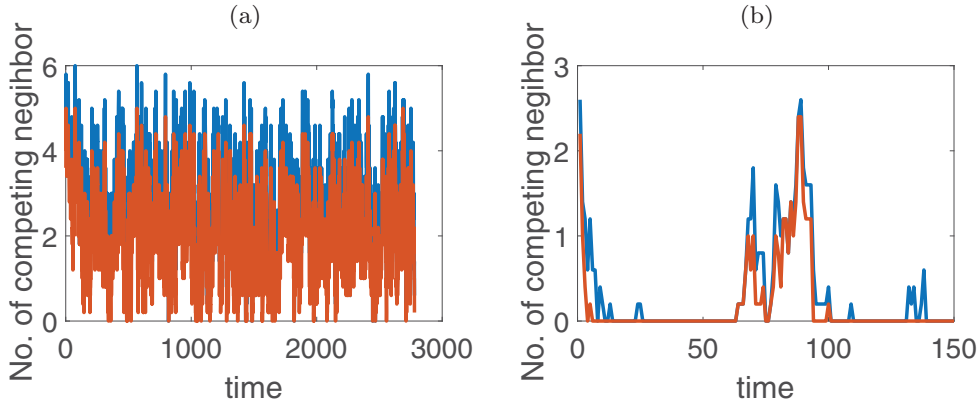

FIG. 2. Average number of neighbors from opposing subgroups for (a) $N_{ui} = 24$ and (b) $N_{ui} = 114$. Different colors correspond to different subgroups. Notice that in the ordered state the two subgroups are segregated from each other.

model; only attraction is required (although the alignment tendency speeds up the decision-making). The basic interactions affecting each self-propelled particle within this model include (i) avoidance of collisions (equivalent to implementing a hard-core repulsion at a unit distance), (ii) attractive interaction which directs particles towards their nearest neighbors (within a distance of six particle sizes), and (iii) alignment of their motion with the average direction of the nearest neighbors. We give the full details of the model in Appendix A.

In this model there is intrinsic noise in the velocity vector of each individual (representing sensory, decision-making, or movement errors), which can lead to an order-disorder transition above a critical noise value [18]. We will restrict our study to the low-noise (ordered) phase, which allows the group to move along the compromise direction when the angular conflict between the two informed subgroups is small ($\theta < \theta_c$) and to achieve consensus above a critical angular difference θ_c. In the disordered regime, for high-intrinsic-noise levels, the group does not move collectively anywhere and thus we cannot study the transition between compromise and decision-making.

Motivated by [10], we vary the number of individuals that exhibit preferred directions of travel as well as those that do not (representing uninformed individuals or those who are informed but do not have a preference regarding where to go), N_{ui}, for a system where the angular conflict is very large (θ close to π). Surprisingly, we find that increasing the number of uninformed members acts to *order* the system and drive it from the compromise to the decision phase. This transition is shown in Figs. 1(b)–1(d), where we see that increasing N_{ui} moves the group from a random-walk motion, described by a unimodal distribution of the flock center-of-mass velocity [Fig. 1(b)], to ballistic motion, which is characterized by a bimodal velocity distribution [Fig. 1(d)]. When the velocity distribution is bimodal [Fig. 1(d)] it represents persistent motion of the group along one of the two preferred directions, which corresponds to a collective decision. When the velocity distribution is localized around $V = 0$ [Fig. 1(b)] the two conflicting informed subgroups cause frequent changes in the direction of group motion and very nearly cancel each other, corresponding to a compromise behavior.

We next explored the role of the extent of angular conflict. This model has been shown to exhibit a transition from averaging to consensus decision-making above a critical angle and it was reported in [10] that the critical angle decreases for a bigger uninformed or unbiased subpopulation. In the phase diagram shown in Fig. 1(e) we see that the system can move from a compromise to a decision state by increasing the number of uninformed members. The transition region is where the velocity distribution changes from unimodal to bimodal and three peaks appear in the velocity distribution. The transition point itself is defined when these three peaks have the same height [see Fig. 1(c)]. We see in Figs. 1(f) and 1(g) that the trajectory of the group is more oriented towards either one of the targets for larger N_{ui}. Increasing N_{ui} has an effect similar to *decreasing* the temperature T in our spin model (discussed below), indicating that the uninformed individuals do not act simply as a source of noise [15].

This effect of the uninformed individuals within the flock model may arise due to their ability to enhance the spatial segregation between the two informed subgroups. This is demonstrated in Figs. 1(f)–1(h), where the degree of spatial segregation is shown to be closely associated with the compromise to decision transition (see also Fig. 2). In Fig. 1(h) we calculate the average distance between members in different subgroups over all pairs and we see that the typical distance increases as time progresses: The simulated groups start with all members mixed, both uninformed and the two informed subgroups. As the group polarizes and starts moving along the direction preferred by one subgroup, the two subgroups separate and the distance between them increases, with the winning subgroup occupying the leading edge and the losing subgroup concentrated at the back. For larger groups this process takes a longer time [Fig. 1(h)], but there exists a higher degree of segregation (normalized separation approaching 1). As the two informed subgroups are more strongly segregated, spatially, it becomes more difficult for the losing subgroup to interact with the winning subgroup and to exert any influence on the motion of the group. This means that the rate at which the velocity changes between the two conflicting directions therefore diminishes once a direction has been selected, which corresponds to a more ordered system (lower effective T). Similarly, the segregation between the subgroups, following the decision transition, is proportionately stronger for larger informed subgroups, even when there are no uninformed individuals [8].

As shown in Fig. 1(i), the separation between the informed subgroups, normalized by the number of uninformed individuals N_{ui}, increases for larger groups. This separation has the characteristics of an order parameter, with a transition towards high segregation above a critical value of N_{ui} [similar to what is shown in Fig. 1(e) for motion towards targets at infinity].

III. SPIN MODEL

The above results of the spatial model of animal groups (flock model) provide us with an ability to describe, using time-consuming computer simulations, behavior that mimics the motion of living groups [6,15]. However, the results of these simulations are rather opaque and do not allow us to gain a deep understanding of the phenomena, especially the sudden transition between averaging preferred directions and deciding among them. It is especially difficult to predict the behavior of the group as a function of the model parameters and to determine which features are general and which are model specific. We therefore propose now an analytically tractable spin model, which allows us to better understand the above behavior.

In animal groups individuals appear to express their preferred direction of motion and affect others predominantly by moving in that direction [6,15]. However, since the group is typically cohesive, it may move in a direction which satisfies the wishes of only one subgroup, while the other subgroups effectively succumb to the collective's choice. Under this condition the losing subgroup has a very weak ability to express its desire to move along a different direction and affect the others, as described in the full spatial model above. We represent these dynamics in the spin model by allowing each informed individual in our model to either exert a social force on the others or not. The rule by which an informed individual switches from exerting a force to relenting is constructed such that an individual is encouraged to exert the force if the group is already moving in that direction. The motion of the group arises from the sum of all exerted social forces and therefore the direction of motion coincides with the force direction. Fast motion along the direction preferred by one subgroup will encourage more members of this subgroup to exert their social force and, on the other hand, depress members from the other (losing) subgroup from exerting a force. We note that in the moving group the social force is often exerted by individuals attempting to move in their preferred direction [6], but social forces exerted by other forms of communication (vocal, for example) can be considered.

This allows us to construct an Ising model for this system, where each informed member is represented by an internal binary state that either applies a force (in a preferred direction) or not. The temperature in our model describes the noise that drives the spin-flipping dynamics and corresponds to the level of individuality of the group members [19,20], whereby higher temperature corresponds to greater individuality, which means a higher tendency to ignore the direction of the group motion and to exert a personal influence. The rules of the model are described in Appendix B. Note that within this minimalist spin model the uninformed individuals are not explicitly described. As already hinted in the discussion of the flock model above, the uninformed or unbiased individuals seem to contribute to the noise and therefore their effect appears in the spin model through the temperature T.

We note that we also explored an alternative spin model, described in Appendix L. In this model the informed individuals always apply a social force in the preferred directions of the two subgroups. We find this model to agree less well with the simulations of the spatial (flock) model described above.

A. Group moving along a line (tug-of-war, $\theta = \pi$)

We start by exploring the dynamics of our model, with the rules as in Appendix B, when the group is moving on a 1D track, where the informed subgroups are pulling towards two targets in opposite directions ($\theta = \pi$). The advantage of this 1D form is that it is an equilibrium model, which therefore allows us to utilize standard thermodynamics and statistical mechanics to extract analytic solutions.

The overall group is of size N, composed of two subgroups of informed individuals of sizes N_1 and N_2 such that $N = N_1 + N_2$. The informed members "pull" the group, somewhat analogously to collective carrying by ants [20]. The model is illustrated in Fig. 3.

Each informed member is described by a spin variable, corresponding to whether it exerts a force $\sigma_i = 1$ or not $\sigma_i = 0$. The order parameter is the 1D velocity of the group V, defined as

$$V = \frac{1}{N}\left(N_1^{(1)} - N_2^{(1)}\right), \tag{1}$$

where $N_{1\,(2)}^{(1)}$ is the number of members that exert a force upward (downward). The system can be described by the Hamiltonian

$$H = -\frac{1}{N}\sum_{i\neq j} J_{ij}\sigma_i\sigma_j, \tag{2}$$

where J_{ij} are the multiplications of the preferred directions of spins i and j such that $J_{ij} = +1$ (ferromagnetic interaction) if they are in the same subgroup and $J_{ij} = -1$ (antiferromagnetic interaction) if they are in competing subgroups. We used here the Kac prescription to allow for a correct thermodynamic limit [21] by normalizing the Hamiltonian by an extra factor of $1/N$ [Eq. (2)] and ignoring finite-size corrections. In the context of the collective motion this normalization arises naturally since the velocity of the group saturates to a finite value when all the individuals align their motion [Eq. (1)]. In certain situations where the individuals do indeed "feel" the combined forces of all the other members in an additive manner [20], one may wish to avoid the normalization by the factor of $1/N$ in Eqs. (1) and (2), which amounts to renormalizing the temperature according to $T \to T/N$ (larger groups are more conformist [20]).

1. Balanced group

We start with the case of two equal-size subgroups ($N_1 = N_2$), which we term the balanced case. Due to the full connectivity of the system (2) the mean-field solution is exact in the infinite-N limit and the equilibrium order parameter for the balanced case is given by the standard Ising form [from Eq. (1)] [22]

$$V = \frac{1}{2}\tanh\left(\frac{V}{T}\right), \tag{3}$$

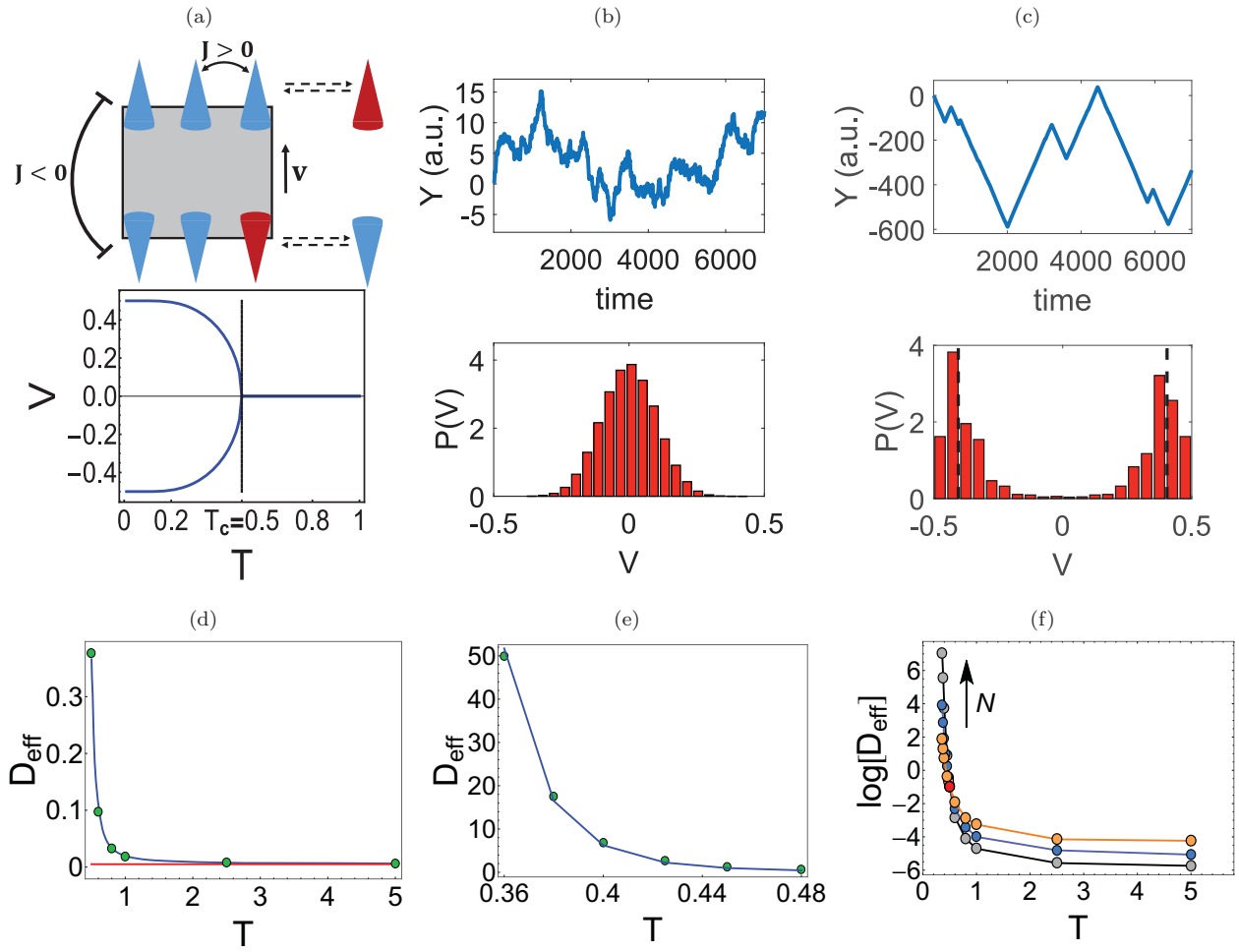

FIG. 3. (a) The upper panel is an illustration of the spin model in one dimension. The triangles represent the informed members in the group. Blue triangles represent the individuals that exert a social force ($\sigma_i = 1$), while the red ones represent individuals that do not exert a force ($\sigma_i = 0$) on the group [Eq. (2)]. Triangles pointing in the same direction are members of the same informed subgroup and tend to encourage each other into the pulling state [ferromagneticlike ($J_{ij} > 0$)], while they tend to suppress the members in the other subgroup into the nonpulling state [antiferromagneticlike interaction ($J_{ij} < 0$)]. In the schematic illustration there is an excess of blue members on the upper side and therefore the group moves in the positive direction, $V > 0$. The lower panel shows stable solutions of Eq. (3). (b) Example of a trajectory for $T = 1 > T_c$ and $N_1 = N_2 = 25$. The motion looks like Brownian motion (top) and the velocity distribution is peaked at $V = 0$ (bottom). (c) Example of a trajectory for $T = 0.36 < T_c$ and $N_1 = N_2 = 25$. The motion looks like a run-and-tumble motion (top) and the velocity distribution is bimodal (bottom). Also shown (as dashed lines) are the solutions of Eq. (3) for $T = 0.36$. (d) Spatial diffusion coefficient for $T > T_c$ ($T_c = 1/2$). Green points are estimated from simulation results. The blue curve is the numerical integration of Eq. (D12) and the red line is $B/2 = (4N)^{-1}$. (e) Spatial diffusion coefficient for $T < T_c$. Green points are estimated from simulation results. The blue curve is Eq. (6), where α is estimated from simulations. (f) Spatial diffusion coefficient in semilogarithmic scale for different system sizes $N = 24, 50, 100$ estimated from simulation data (lines are guides to the eye). The diffusion coefficient at the critical point ($T_c = 1/2$) is denoted by the red point and it has the same value for all the sizes [Eq. (D13)].

where T is the temperature. For $T > T_c = 1/2$ Eq. (3) has only the solution $V = 0$ [Fig. 3(a), lower panel], which means that the steady-state motion of the group is diffusive, and this corresponds to the compromise state of the group. For $T < T_c$ there are only stable solutions with positive and negative signs $V = \pm V_0(T)$. This is the ordered regime where the group is moving with a well-defined mean speed along the direction preferred by one of the informed subgroups, which corresponds to the decision state of the group. We therefore identify T_c with the temperature of the decision transition.

We plot typical group trajectories for the balanced case for both high [Fig. 3(b)] and low [Fig. 3(c)] T. The resulting motion looks diffusive for high T and run-and-tumble for low T. Note that although the run-and-tumble motion is ballistic on short time scales, on long time scales it is also diffusive. We therefore analyze the motion performed by the group by calculating the effective spatial diffusion coefficient $D_{\rm eff}$ for all temperature regimes. For $T > T_c$ we write the Langevin equation, expanding Eq. (3) up to cubic order in V (since the average V is small),

$$\frac{dV}{dt} = -\gamma(T)V - \frac{V^3}{6T^3} + \sqrt{B}\eta(t), \tag{4}$$

where $\gamma(T) = (T - T_c)/T$, the noise term is given by [see Appendix C for a derivation of Eqs. (4) and (5)]

$$B(V) = \lim_{\delta t \to 0} \frac{\langle \delta V^2 \rangle}{\delta t} = \frac{1}{N}\left[\frac{1}{2} - (V - h)\tanh\left(\frac{V}{T}\right)\right], \quad (5)$$

and $\eta(t)$ is the white Gaussian noise: $\langle \eta(t)\eta(t')\rangle = \delta(t - t')$. Note that the time is effectively renormalized by the basic rate of individual decision-making, i.e., the rate of spin flips.

From the Langevin equation (4) we can calculate the effective diffusion coefficient of the group for long times, using the Kubo integral [23,24] (see Appendix D for details). In the limit $T \gg T_c$ we get the expected result of the Einstein relation [25], namely, $D_{\text{eff}} = B(2\gamma^2)^{-1} = T^2[4N(T - T_c)^2]^{-1}$, where $B = (2N)^{-1}$ plays the role of the temperature for the real-space Brownian motion of the group.

At $T = T_c$, where $\gamma = 0$, we are left only with cubic friction in Eq. (4). We find that at T_c the diffusion coefficient has a value that is independent of the system size N, due to the scale invariance of the critical state. The diffusion was shown to be independent of the noise intensity (which in our case is given by the N-dependent B) for cubic friction [26]. We compare the diffusion coefficient extracted from linear fits to the mean-square displacements from simulations to the analytic expression [which is calculated in Eq. (D12)] in Fig. 3(d) to find a very good agreement for all $T > T_c$. We see that D_{eff} is smaller for bigger systems in the compromise phase ($T > T_c$) since the effect of fluctuations is weaker for bigger systems (stronger cancellations) and therefore the velocity fluctuates less, leading to a velocity distribution that is more tightly localized around the average value of $\langle V \rangle = 0$.

For $T < T_c$ the motion changes from simple diffusion to a run-and-tumble motion, where the group moves with a constant velocity magnitude $|V| = V_0$ and switches direction stochastically. We define $\alpha(T)$ as the rate of jumping between the two symmetric solutions of Eq. (3), $\pm V_0(T)$. On long time scales the diffusion coefficient for $T < T_c$ is given by

$$D_{\text{eff}}(T) = \frac{V_0(T)^2}{2\alpha(T)}. \quad (6)$$

We derive this result from the general result calculated in Appendix E. We extract both $V_0(T)$ and $\alpha(T)$ from the simulations and then insert these values into Eq. (6). In Fig. 3(e) we see that Eq. (6) gives the correct values of the effective diffusion coefficient. The tumble rate $\alpha(T)$ was extracted from the simulations using the decay time of the velocity-velocity temporal correlations. For $T \ll T_c$ we find that $\alpha(T)$ can be described analytically as it converges to the Kramers escape rate (see Appendix G and Fig. 8).

As shown in Fig. 3(e), in the decision phase ($T < T_c$), the diffusion D_{eff} *increases* with group size, since the effect of fluctuations is weaker for bigger systems (stronger cancellations), and therefore the velocity fluctuates less, leading to a velocity distribution that is more tightly localized around the average value of $\langle V \rangle = \pm V_0$, resulting in fast ballistic motion.

2. *Imbalanced group*

If the subgroups are of different sizes ($N_1 \neq N_2$) we use the term *imbalanced* case. For $N_1 > N_2$ we get [Eq. (1)]

$$V = \frac{1}{2}\tanh\left(\frac{V}{T}\right) + h, \quad (7)$$

where $h = (N_1 - N_2)/2N$. We see from Eq. (7) the existence of a majority and a minority translates in the Ising framework to an effective external magnetic field. For large T we obtain the average velocity by expanding Eq. (7) up to cubic order

$$-\gamma(T)V - \frac{1}{6}\left(\frac{V}{T}\right)^3 + h = 0. \quad (8)$$

For $T \gg T_c$ we find a linear response $V = h/\gamma(T) = Th/(T - T_c)$, while at $T = T_c$ we get a nonlinear response $V = (3h/4)^{1/3}$. For $T < T_c$ we numerically solve Eq. (7) [see the comparison with simulations in Fig. 4(a)]. Below a temperature $T^* < T_c$ a metastable solution appears, with V having an opposite sign to h. This T^* is given by [from Eq. (8)]

$$T^* = T_c - \left(\frac{3h}{2\sqrt{2}}\right)^{2/3}. \quad (9)$$

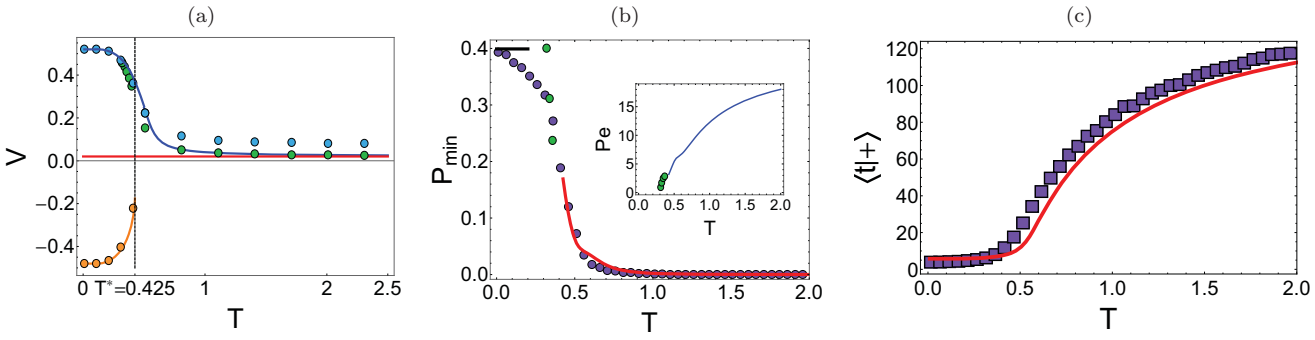

FIG. 4. (a) Velocity of the imbalanced group ($N_1 = 26, N_2 = 24$) vs the temperature. Solid curves correspond to solutions of Eq. (7). The circles are results obtained from simulations: Blue (yellow) circles give the average positive (negative) velocity, while green circles represent the average velocity. The vertical dashed line is T^* [defined in Eq. (F6)]. The red line is the bias term $h = (N_1 - N_2)(2N)^{-1} = 0.02$. (b) Minority probability for $L = 6$. Purple circles are the results of simulations. The red curve ($T > T^*$) and green circles ($T < T^*$) are P_{min} of Eq. (12). The inset shows the corresponding Péclet number [Eq. (10), using Eqs. (7) and (D10)]. (c) Conditional mean first-passage time for $L = 6$. Purple squares are simulation results while the red curve is Eq. (13).

Note that in the imbalanced case, as in an Ising model with an external magnetic field, we do not have a phase transition, since the symmetry between the two subgroups is already broken. Even at high temperature ($T > T_c$) we have a decision, in the sense that the group always drifts in the majority direction. The diffusion coefficient of the group can also be calculated for the imbalanced case, as calculated in Appendixes E and F and shown in Fig. 9.

3. Accuracy and time to reach the target

We now wish to analyze the process whereby the group reaches targets that are at some finite distance from the initial position (along the 1D line). In general, we take the initial position at $x = L/2$, while the two targets are at $x = 0, L$. We are interested in finding the probability of reaching the majority vs the minority targets, as well as the average time it takes to complete the trajectory. These quantities are shown in Figs. 4(b) and 4(c), i.e., the probability of reaching the minority target and the conditional mean time to reach the majority target, $\langle t|+\rangle$, respectively.

We start with Fig. 4(b), where we find that for $T < T_c$ there is a large probability for the group to reach the minority target. In order to explain this behavior we investigate the system with respect to the dimensionless Péclet number, which allows us to characterize the conditions when we expect the imbalance to dominate the motion, which means that the group reaches the majority target with high probability. On the other hand, when the diffusion is dominant, the group can reach the minority target with large probability too. The Péclet number is the ratio between the diffusion time and the time it takes the system to drift towards the majority target. This ratio is given by

$$\mathrm{Pe} = \frac{L^2/D_{\mathrm{eff}}}{L/V} = \frac{VL}{D_{\mathrm{eff}}}. \tag{10}$$

When $\mathrm{Pe} \ll 1$ the trajectory is dominated by diffusion, while for $\mathrm{Pe} \gg 1$ the imbalance dominates the behavior. We can say that the transition between imbalanced and diffusive random walks occurs roughly at $\mathrm{Pe} = 1$.

In light of the Péclet number we can understand qualitatively the decision that the group makes [Fig. 4(b)]. For high enough $T > T_c$, we find that D_{eff} is inversely proportional to the group size N [Fig. 3(f)], so it is small compared to VL for large L, N. Therefore, from Eq. (10), $\mathrm{Pe} \gg 1$, which means that the system is dominated by the imbalance and will reach the majority target with high probability. For low $T < T_c$, D_{eff} is large and therefore $\mathrm{Pe} \ll 1$. This suggests that the behavior is dominated by diffusion, which gives the minority a finite probability of winning. Furthermore, we expect the minority probability to start increasing when $\mathrm{Pe} \simeq O(1)$. If we increase the separation between the targets L, the Pe is increased such that the minority probability starts to increase at lower T. These qualitative predictions are verified in Fig. 5.

We quantify the probability of reaching either target as follows. Let $c(x,t)$ be the probability density to find the group at location x at time t. If the group performs an imbalanced

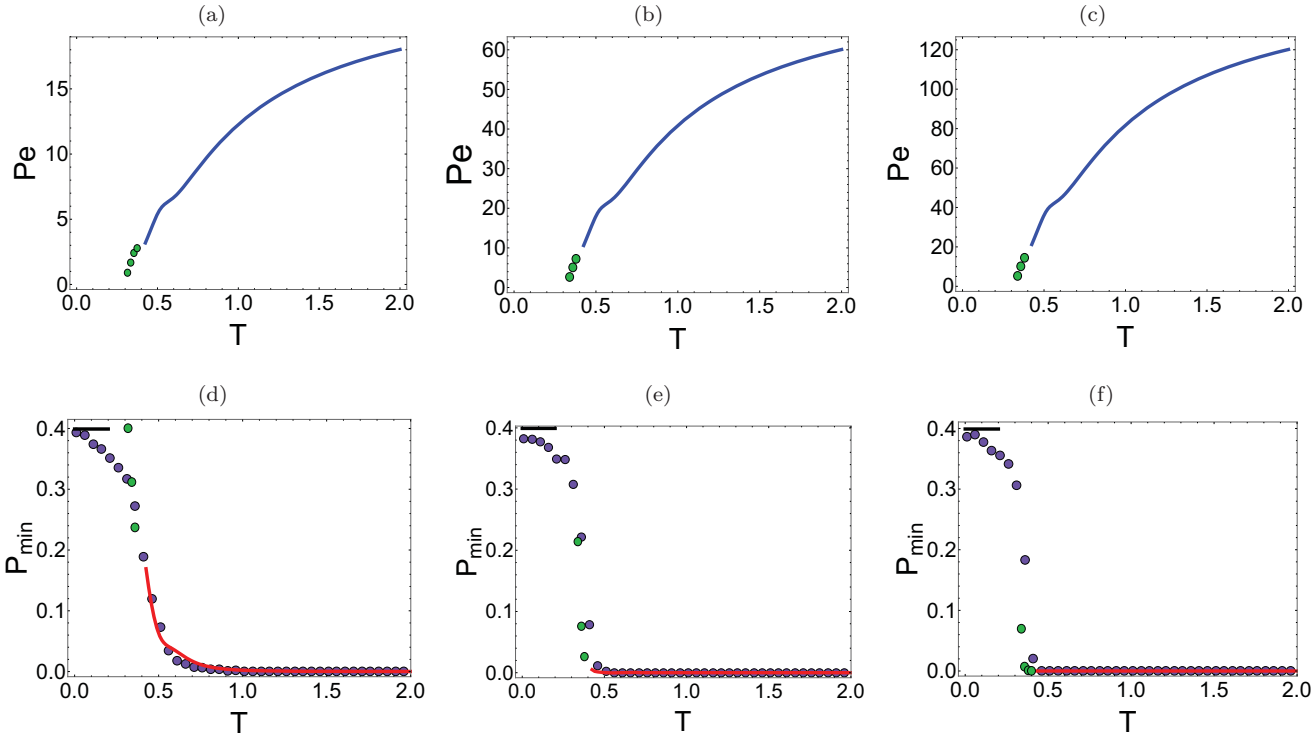

FIG. 5. Péclet number for (a) $L = 6$, (b) $L = 20$, and (c) $L = 40$. The system parameters are as in Fig. 3. The blue curve is a calculation using Eqs. (7) and (10) for $T > T^*$. The green circles are estimated from simulations for $T < T^*$. Also shown are the corresponding minority probabilities for (d) $L = 6$, (e) $L = 20$, and (f) $L = 40$. Purple circles are the results of simulations. The red curve ($T > T^*$) and green circles ($T < T^*$) are P_{min} of Eq. (12), using for Pe the calculation given by the blue line or the green circles in (a)–(c), respectively. The horizontal black line is the estimation of P_{min} for $T \to 0$ shown in Eq. (H5).

random walk its behavior is determined by the equation

$$\frac{\partial c(x,t)}{\partial t} = D_{\text{eff}}\frac{\partial^2 c(x,t)}{\partial x^2} - V\frac{\partial c(x,t)}{\partial x}, \tag{11}$$

where the mean drift velocity V and effective diffusion coefficient D_{eff} were calculated in the preceding section.

The two targets found at 0 and L are incorporated into Eq. (11) as absorbing boundary conditions $c(0,t) = c(L,t) = 0$ and the initial condition is that the group is in the middle: $c(x,0) = \delta(x - L/2)$. We follow the electrostatic analogy as described in [27] to calculate the probability to exit from each target as the integrated current at that position

$$P_{\text{maj}} = \frac{1 - e^{-VL/2D_{\text{eff}}}}{1 - e^{-VL/D_{\text{eff}}}} = \frac{1 - e^{-\text{Pe}/2}}{1 - e^{-\text{Pe}}},$$
$$P_{\text{min}} = \frac{e^{-VL/2D_{\text{eff}}} - e^{-VL/D_{\text{eff}}}}{1 - e^{-VL/D_{\text{eff}}}} = \frac{e^{-\text{Pe}/2} - e^{-\text{Pe}}}{1 - e^{-\text{Pe}}}, \tag{12}$$

where $P_{\text{maj (min)}}$ corresponds to the majority (minority) target.

Comparing these analytic expressions with the simulations, we see in Fig. 4(b) that for $T > T^*$ (and $L/2 \geqslant 3$) Eq. (12) gives a good approximation (see also Fig. 5). For $T < T^*$ (or for $L/2 < 3$) the approximation gives a significant discrepancy compared to the simulations. This discrepancy suggests that Eq. (12) is not valid for small Péclet number (small T and L). An example of this discrepancy is the $T \to 0$ (Pe $\to 0$) limit where Eq. (12) predicts $P_{\text{min}} \to 0.5$, which is different from the observation.

The discrepancy we find at $T < T^*$ arises due to the dominance of the initial conditions in determining the final destination. In the limit of $T \to 0$ we derive the probability of reaching the minority based on the initial configurations of the spins (see Appendix H). The result can only be calculated numerically, and in Fig. 4(b) we show that indeed the minority probability converges to this result (see also Fig. 5).

Finally, we calculate the conditional mean time it takes to get to the majority target $\langle t|+\rangle$. In the limit $T \to 0$ we expect a ballistic behavior; therefore, the mean travel time is given by

$$\langle t|+\rangle = \frac{L}{2V(T)}. \tag{13}$$

Indeed, we see in Fig. 4(c) that the mean travel time converges to this result at low T.

For high $T > T_c$ we expect an imbalanced motion (drift) towards the majority target. This motion is, on average, with speed $V(T)$, so we again expect the relation (13) to apply. Therefore, it seems that the conditional mean first-passage time is given in general by this expression for all T, as shown in Fig. 4.

We note that the results of Figs. 4(b) and 4(c) suggest that there may be an optimal temperature with respect to minimizing both the chances of reaching the minority target and the time taken to reach the target. The trade-off between these two quantities is clear from Eqs. (10) and (13), which depend on $V(T)$ in the opposite manner.

B. Group moving in two dimensions (arbitrary θ)

1. Fixed angular conflict (targets at infinity)

We now wish to study within our spin model a system that is not constrained to move on a line but free to move in a 2D plane. For the balanced case, each of the two equal subgroups has a different preferred direction, differing by an angle $\theta \leqslant \pi$ [Fig. 6(a)]. In this case the spins in the different informed subgroups have an overlapping component in the direction along the angle bisector. This means that when there is no decision to go along one of the preferred directions, the compromise will result in motion along this angle bisector.

As long as the two subgroups maintain fixed preferred directions, i.e., the targets are infinitely far away, the system is described by a time-independent Hamiltonian and is amenable to an equilibrium description. The Hamiltonian of the system is

$$H = -\frac{1}{N}\sum_{i\neq j}\hat{p}_i \cdot \hat{p}_j \sigma_i \sigma_j, \tag{14}$$

where $\hat{p}_i$ denotes the preferred directions of the two subgroups

$$\hat{p}_1 = \cos\left(\frac{\theta}{2}\right)\hat{x} + \sin\left(\frac{\theta}{2}\right)\hat{y},$$
$$\hat{p}_2 = \cos\left(\frac{\theta}{2}\right)\hat{x} - \sin\left(\frac{\theta}{2}\right)\hat{y}. \tag{15}$$

Within each subgroup the dot product $\hat{p}_i \cdot \hat{p}_j$ is positive and therefore the interaction is ferromagnetic. However, the interaction between members from different subgroups is antiferromagnetic if $\theta > \pi/2$ or ferromagnetic if $\theta < \pi/2$.

We wish to solve the mean velocity of the system along the y direction, which is the direction of the conflict, i.e., $V_y = \frac{1}{N}\sum_i \hat{p}_i \cdot \hat{y}\sigma_i$. Using the equilibrium distribution of the system in the limit of $N \gg 1$, we get an effective free energy in terms of the order parameter V_y (see Appendix I). We can expand this free energy as

$$\mathcal{G}_{\text{eff}} = \frac{a}{2}(V_y)^2 + \frac{b}{4}(V_y)^4. \tag{16}$$

The system has two phases: a high-T phase characterized by $V_y = 0$ and a low-T phase with $V_y \neq 0$, while $V_x \neq 0$ for every T. In Figs. 6(b) and 6(c) we plot examples of the minima of the free energy $\mathcal{G}_{\text{eff}}$, which denote the direction in which the group moves, as a function of the conflict angle θ. We find that the group can undergo both a second-order and a first-order transition, depending on the temperature. These results, including the case of imbalance between the subgroups (see Appendix J and Fig. 11 for more details), are in excellent agreement with previous results obtained from spatial simulations of animal groups [8].

We plot in Fig. 6(d) the phase diagram of the system as a function of T and θ. The curve $a = 0$ [Eq. (16)] defines the second-order transition curve, as long as $b > 0$. At the tricritical point T_3, $(a = 0, b = 0)$, the transition changes its nature to first order. For $T < T_3$ the transition is first order. As in the previous section, $T_c = 1/2$ is the critical temperature at $\theta = \pi$, so if $T > T_c$ no transition is possible. For $\theta < 2\pi/3$ we find that there is no decision phase, even in the limit of $T \to 0$.

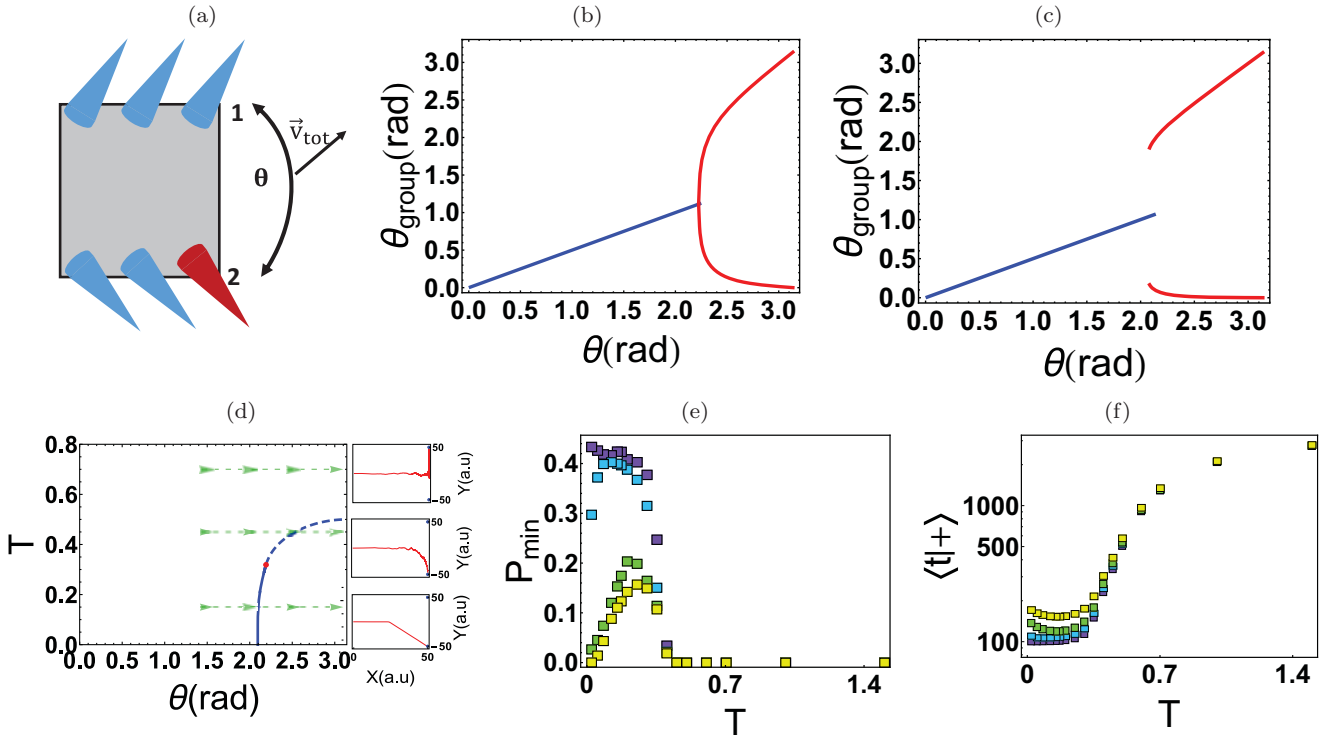

FIG. 6. (a) Illustration of the 2D spin model. Active spins are represented as blue members and inactive spins as red members. The angular difference between the two subgroup orientations is θ. In the figure, subgroup 1 exerts a stronger force. (b) and (c) Calculated minima of the free energy $\mathcal{G}_{\text{eff}}$ [Eq. (16)], which denote the group's direction of motion (we take here the direction of group 2 to be along 0°), for (b) $T = 0.35$ (second-order transition) and (c) $T = 0.2$ (first-order transition). The blue curve is the compromise solution, while decision curves are in red. (d) Phase diagram for a group moving in two dimensions. The blue dashed line is the second-order transition curve while the blue solid curve is the first-order transition curve with the tricritical point denoted by a red point. On the right are example trajectories for a symmetric group with $N_1 = N_2 = 15$ and targets located at $X = 50$ and $Y = \pm 50$ for (from top to bottom) $T = 0.7, 0.45, 0.15$. Trajectories correspond to moving on the green lines in the phase diagram. (e) Probability of reaching the minority target located at $Y = -50$ and $X = 10$ (purple), $X = 20$ (blue), $X = 30$ (green), and $X = 50$ (yellow). (f) Average time to reach the majority target. Colors are as in (e).

Note that our spin model can be used to explore conflicts between a larger number of biased subgroups. For example, three-way conflicts [28] can also be explored and the corresponding compromise-decision phase diagram exposed (see Appendix M, Fig. 13).

2. *Fixed targets at a finite distance*

We now wish to explore the motion of the group in two dimensions, where the targets are fixed. We give the details of the simulation in Appendix K. As the two subgroups are always oriented towards the targets, their desired directions $\hat{p}_1$ and $\hat{p}_2$ depend on the instantaneous position of the group and therefore vary with time. The connectivity is $J_{ij} = \hat{p}_i \cdot \hat{p}_j$ [see Eq. (14)], so the Hamiltonian is now time dependent and the system is no longer in equilibrium.

For large $T \gg T_c$, the system does not undergo a decision transition [Fig. 6(d)] and the trajectories have a ballistic motion of the group until it reaches the line connecting the two targets ($X = 0$), where $\theta \simeq \pi$. The group continues by diffusion towards one of the targets. At low T the motion is again ballistic towards the $X = 0$ line, but there is a point along the motion where, as the targets are approached, the critical angle is inevitably reached and a transition occurs, and one subgroup wins over the other. If T is very low, this choice is practically irreversible, while at temperatures just below T_c there can be several switches in direction.

We next explore the 2D motion of imbalanced groups $N_1 \neq N_2$. We see in Fig. 6(e) that when the group starts the motion at an angle that is larger than $\theta_c(T)$, the behavior is similar to the 1D case [Fig. 2(b)] and the probability for the minority's success is increasing monotonically as T decreases. However, when the group starts at a smaller initial angle [$\theta < \theta_c(T)$], we find that the probability of reaching the minority target abruptly vanishes at $T \to 0$. The reason behind this new regime is the following: When the system is moving in the compromise regime, the two subgroups enhance each other, which enables the majority group to give a small drift velocity in its preferred direction. When the system then crosses the critical angle, this small drift velocity biases the decision in the majority's direction. When the temperature is now increased, this small bias that the majority produced during the compromise motion is eliminated by the larger noise, leading to an increase in the probability to reach the minority-preferred direction. At even higher temperatures the system behaves again as in the 1D case, since it reaches the line joining the two targets before any decision (if at all) is made.

As in one dimension [Figs. 3(b) and 3(c)], the 2D results suggest a trade-off in the group decision-making process,

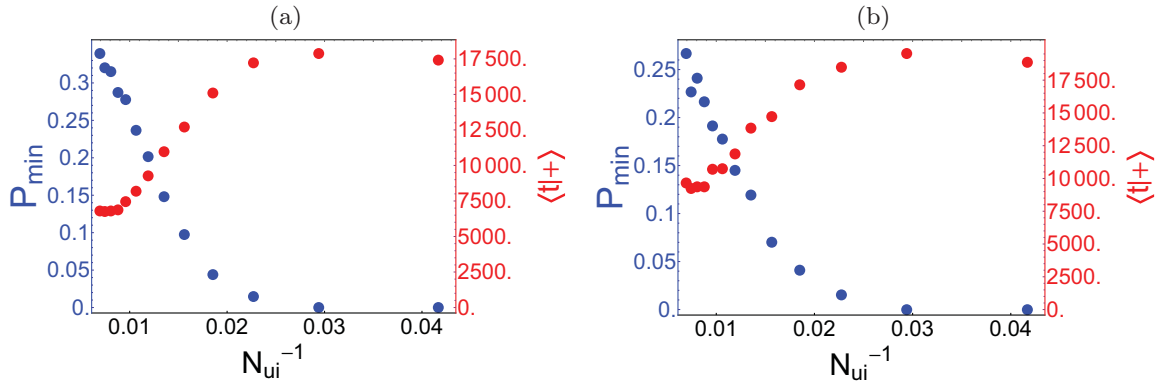

FIG. 7. Trade-off with $N_1 = 6$, $N_2 = 5$, and $\omega = 0.3$. The locations of the targets compared to the group's initial position are (a) $(X = 0, \Delta Y = 500)$ and (b) $(X = 250, \Delta Y = 500)$.

measured by the time taken (distance moved) to reach the majority target, and the accuracy of the decision. For low T, the group reaches a decision quickly, making the travel time and path length very short. As in natural settings, animal groups are exposed to both predation and competition for resources, making fast decision-making important for survival. However, low T also implies the existence of metastable states in the system, which allows the minority subgroup to strongly affect the outcome. Assuming that the majority is more likely to have the correct (better) information, there may be selection against the minority-wining scenario. Therefore, to minimize the combined costs of travel time and accuracy, selection may be such that groups may exhibit an effective T of intermediate values when starting with a large conflict angle θ. When the group starts with a compromise state, for small initial θ, we find that at very low T both the accuracy is high (low probability of reaching the minority target) and the travel time is low. This is therefore the "optimal" regime when groups have a long initial trajectory along the compromise direction, before the conflict gives rise to the decision transition. In order to achieve this low-T window, which minimizes both the errors and travel time, the group needs to have access to the information about the targets at very large distances. This may be the case for migrations or when individuals remember distant foraging areas, but may not always be possible and could also be costly in terms of time and energy resources.

C. Comparison between the spin and flock models

The spin model results for motion in two dimensions, such as the phase diagram and the trajectories shown in Fig. 6(d), resemble qualitatively the results we obtained using the flock model [Figs. 1(e)–1(g)]. The role of temperature in the spin model is analogous to the inverse of the number of uninformed (unbiased) individuals in the flock model. However, to demonstrate the applicability of our spin model, we tested if the trade-off we found in the spin model between accuracy and travel time as a function of temperature is found also in the flock model.

For this comparison, we recall that increasing N_{ui} has an effect similar to *decreasing* the temperature T in our spin model [compare Figs. 1(e) and 6(d)]. Note that when there are no uninformed individuals ($N_{ui} = 0$), there is still a finite effective temperature T that can be associated with the mapping between the spin model and the flock model and this T also decreases for larger flocks, i.e., flocks with larger informed subgroups [8].

We tested the trade-off between accuracy and efficiency using the flock model when the angular difference between targets is 180°; this setting corresponds to the 1D process of Sec. III A. Figure 7(a) shows results which are similar to the trade-off in one dimension for the spin model [see Figs. 4(b) and 4(c)]. As can be seen in Fig. 7(b), the trade-off that we found for the 2D spin model [Figs. 6(e) and 6(f)] is manifested also in the full flock model, demonstrating the impact of the metastable minority state at low temperature (large N_{ui}).

Note that in [15] the probability of the minority's success was studied in a regime of small groups, with a more persuasive minority. In this regime, with a very small uninformed population, increasing the number of unbiased individuals was found to actually facilitate the majority decision. A similar trend is shown in Fig. 8 for the spin model when the minority subgroup applies a stronger social force per individual. The probability of reaching the minority target decreases with

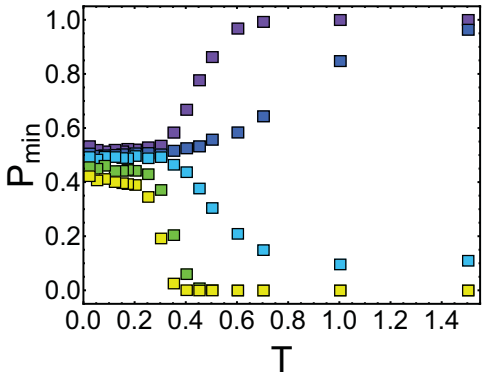

FIG. 8. Probability of reaching the minority target located at $Y = -50$ and $X = 10$, starting at $(X,Y) = (0,0)$ but with different intrinsic forces for the individuals within the two groups. Here $N_{maj} = 11$, $N_{min} = 10$, and, from bottom to top, $\beta = \frac{f_{min}}{f_{maj}} = 1, 1.05, 1.1, 1.11, 1.13$.

decreasing T, which corresponds to a larger uninformed population.

IV. DISCUSSION

We have presented a simple spin model which is analytically tractable and describes the basic features of the decision transition observed for moving animal groups. This model allows us to calculate the decision transition phase diagram and to make predictions which we then corroborated using simulations of a detailed flock model, regarding the trade-off between speed and accuracy of the group motion. An advantage of our spin model is that unlike the flock models that are inherently out of equilibrium, our model is in thermal equilibrium (for the case of preferred directions rather than localized targets). This allows us to investigate which properties of the decision transition dynamics arise from nonequilibrium rather than equilibrium aspects of the system.

Unlike previous attempts to model group decision-making and social behavior using spin models [11,19,29,30] where the spin degree of freedom represented only the direction of motion chosen by the individual, the spin degree of freedom in our model describes the state of the individual, i.e., whether that individual applies a social force or not.

We find that the role played by noise (temperature) in our spin model is analogous to the inverse of the number of uninformed individuals in the flock model. This correspondence could be related to the observations that individuals tend to behave in a more conformist manner in larger groups [20]. In addition we find that, as a function of the temperature (and therefore the number of uninformed individuals in the flock), there is a trade-off between the speed with which the group can reach a target and the probability that the majority-preferred target will be the one selected (based on the available information). This trade-off could drive the evolution of social animals to optimize their group size and interaction strength. Our simple spin model allows us to explore the collective decision-making process in more complex regimes and environments, without resorting to costly simulations of spatial flock models, as well as provide analytical solutions that give deeper understanding.

We note that our model may serve as a basis for the description of other forms of collective decision-making phenomena, in cellular, animal, and under some circumstances possibly even human groups. For example, our results may indicate that a high level of individuality (such that $T > T_c$) can ensure that the majority target is reached, although there are frequent changes of the global direction of motion. On the other hand, at low temperature (high conformity) there is a larger probability for the minority to gain the upper hand, which may be detrimental. A similar analogy between temperature and the inverse of the system's size has been found in [20] for collective transport by ant groups, in genetic population models [31], and in ecological models [32].

It is tempting to draw an analogy between our model and models for decision-making in the brain [33]: The instantaneous group velocity plays the role of the firing rate of the neurons and the group's position is the integrated firing rate. We can therefore propose that the sizes of neuronal groups and their intrinsic noise levels may be optimized in networks that control decision-making processes. This analogy may be further explored in the future. Examples of future extensions of our model may include making the strength of the social forces dependent on the individual's history as well as giving each individual more than two choices (i.e., described by spins of higher order).

ACKNOWLEDGMENTS

The research of N.S.G. was supported by the ISF (Grant No. 580/12). This research was made possible in part by the generosity of the Harold Perlman family. N.S.G. is the incumbent of the Lee and William Abramowitz Professorial Chair of Biophysics. I.D.C. acknowledges support from the NSF (Grant No. IOS-1355061), the ONR (Grants No. N00014-09-1- 1074 and No. N00014-14-1-0635), the ARO (Grants No. W911NG-11-1-0385 and No. W911NF-14- 1-0431), the Human Frontiers Science Program (Grant No. RGP0065/2012), the Struktur- und Innovationsfunds für die Forschung of the State of Baden-Württemberg, and the Max Planck Society.

APPENDIX A: RULES OF THE SPATIAL FLOCK MODEL

The ith particle's location is $\vec{c}_i$ and its direction of motion $\vec{v}_i$. The direction of motion for each agent is updated with the following steps: The first step is avoidance from other members; if $\vec{d}_i$ is the desired direction, it becomes, after this step,

$$\vec{d}_i(t+dt) = -\sum_{j\neq i} \frac{\vec{c}_j(t) - \vec{c}_i(t)}{|\vec{c}_j(t) - \vec{c}_i(t)|}, \tag{A1}$$

where $\vec{d}_i$ represents the chosen direction if avoidance was the only interaction. The sum is taken over particles in a radius $\alpha = 1$ around particle i. The next step occurs only if there are no particles inside the radius α. These are the attraction and alignment interactions

$$\vec{d}_i(t+dt) = \sum_{j\neq i} \frac{\vec{c}_j(t) - \vec{c}_i(t)}{|\vec{c}_j(t) - \vec{c}_i(t)|} + \sum_j \frac{\vec{v}_j(t)}{v_j(t)}, \tag{A2}$$

where the sum is over particles in radius $\rho = 6$ around particle i. Normalizing the direction $\hat{d}_i = \vec{d}_i/d_i$ and taking the information into account, we get

$$\tilde{d}_i = \frac{\hat{d}_i + \omega\hat{p}}{|\hat{d}_i + \omega\hat{p}|}, \tag{A3}$$

where $\hat{d}_i$ is the direction chosen after taking into account the repulsion, alignment, and attractive interaction; ω is the weight of the information so $\omega = 0$ ($\neq 0$) for uninformed (informed) agents; and $\hat{p}$ is the direction of the informed members and is defined as in Eq. (15). In this work we set $\omega = 0.3$ for the informed members.

APPENDIX B: DYNAMICS OF THE SPIN MODEL

We chose the dynamics of the system to follow Glauber dynamics [34]. The rate for jumping between states l and k is

$$r_{l\to k} = \frac{1}{1+\exp\left(\frac{\Delta H_{lk}}{T}\right)}, \tag{B1}$$

where ΔH_{lk} is the energy difference between the two states with the Hamiltonian (2). In the thermodynamic limit of $N \gg 1$ we can write the individual spin-flip rates as a function of the order parameter V, defined in Eq. (1),

$$r^{(1)}_{1\to 0} = \frac{1}{1+\exp\left(\frac{2V}{T}\right)}, \quad r^{(2)}_{1\to 0} = \frac{1}{1+\exp\left(-\frac{2V}{T}\right)},$$
$$r^{(1)}_{0\to 1} = \frac{1}{1+\exp\left(-\frac{2V}{T}\right)}, \quad r^{(2)}_{0\to 1} = \frac{1}{1+\exp\left(\frac{2V}{T}\right)}, \tag{B2}$$

where the upper index 1 or 2 denotes the subgroup (1 pointing upward and 2 downward) and the lower index 0 or 1 denotes the spin state. By defining the rates in this manner we have rescaled time in units of the basal decision-making frequency. Therefore, the mean of V for a imbalanced walker has the dynamics [35]

$$\frac{dV}{dt} = -V + \frac{1}{2}\tanh\left(\frac{V}{T}\right) + h. \tag{B3}$$

APPENDIX C: EQUATIONS OF MOTION FOR VELOCITY MOMENTS

In this section we derive Eqs. (4) and (5). We begin by looking at the system at a very small time interval δt such that at most there can be only one event. We define the instantaneous change in the velocity as δV and it takes values of

$$\delta V = \begin{cases} +1/N, & P_+ = r_+\delta t \\ -1/N, & P_- = r_-\delta t, \end{cases} \tag{C1}$$

where P_+ and P_- are the probabilities for each value and r_+ and r_- are the rates at which each value occurs. Equation (4) is computed from

$$\frac{d\langle V\rangle}{dt} = \lim_{\delta t\to 0}\frac{\langle \delta V\rangle}{\delta t} = \lim_{\delta t\to 0}\frac{P_+ - P_-}{N\delta t} = \frac{r_+ - r_-}{N}. \tag{C2}$$

The rates are given by

$$r_+ = N^{(0)}_1 r^{(1)}_{0\to 1} + N^{(1)}_2 r^{(2)}_{1\to 0},$$
$$r_- = N^{(1)}_1 r^{(1)}_{1\to 0} + N^{(0)}_2 r^{(2)}_{0\to 1} \tag{C3}$$

and by using $N_1 = N^{(0)}_1 + N^{(1)}_1 = N/2 + Nh$ [recall that $h = (N_1 - N_2)(2N)^{-1}$] and Eqs. (B2) we get

$$r_+ = \left(\frac{N}{2} + Nh - N^{(1)}_1 + N^{(1)}_2\right)\frac{1}{1+e^{-2V/T}},$$
$$r_- = \left(\frac{N}{2} - Nh + N^{(1)}_1 - N^{(1)}_2\right)\frac{1}{1+e^{2V/T}}. \tag{C4}$$

Substituting the rates in Eq. (C2) and using $V = (N_1 - N_2)(2N)^{-1}$ yields

$$\frac{d\langle V\rangle}{dt} = \frac{1}{2}\left(\frac{1}{1+e^{-2V/T}} - \frac{1}{1+e^{2V/T}}\right) + h - V$$
$$= \frac{1}{2}\tanh\left(\frac{V}{T}\right) + h - V \tag{C5}$$

and by approximating $\langle V\rangle \approx V$ we get the equation for the average velocity.

We now develop Eq. (5). From Eq. (C1) we see that

$$\langle \delta V^2\rangle = \frac{P_+ + P_-}{N^2} \tag{C6}$$

and therefore

$$B(V) = \lim_{\delta t\to 0}\frac{\langle \delta V^2\rangle}{\delta t} = \frac{r_+ + r_-}{N^2}. \tag{C7}$$

Using the rates from Eq. (C4), we get Eq. (5).

APPENDIX D: CALCULATION OF DIFFUSION COEFFICIENT: BALANCED CASE

In this appendix we describe briefly the calculation in [24]. Consider the Langevin equation

$$\frac{dV}{dt} = F(V) + \sqrt{B}\eta(t), \tag{D1}$$

where $\langle \eta(t)\eta(t')\rangle = \delta(t-t')$. We describe how to calculate the effective diffusion coefficient $D_{\rm eff}$. The corresponding Fokker-Planck equation of the Langevin equation is

$$\frac{\partial W(V,t)}{\partial t} = -\frac{\partial F(V)W(V,t)}{\partial V} + \frac{B}{2}\frac{\partial^2 W(V,t)}{\partial V^2}$$
$$= L_{\rm FP}W(V,t), \tag{D2}$$

where $W(V,t)$ is the probability density of V at time t and in the second line we wrote the equation with the Fokker-Planck operator. The diffusion coefficient is given by the Kubo formula

$$D_{\rm eff} = \int_0^\infty dt\langle V(0)V(t)\rangle. \tag{D3}$$

The autocorrelation is given by

$$\langle V(0)V(t)\rangle = \iint VV'W(V,t;V',0)dVdV'$$
$$= \int Ve^{L_{\rm FP}(V)t}VW_{\rm st}(V)dV = \int V\omega(V,t)dV, \tag{D4}$$

where $W_{\rm st}$ is the stationary probability distribution of V. We then insert this result in Eq. (D3),

$$D_{\rm eff} = \int_0^\infty dt\int_{-\infty}^\infty dV\, V\omega(V,t)$$
$$= \int_{-\infty}^\infty dV\, V\int_0^\infty dt\,\omega(v,t) = \int_{-\infty}^\infty dV\, V\rho(V). \tag{D5}$$

Since $\omega(V,t) = e^{L_{\rm FP}(V)t}VW_{\rm st}(V)$ it is evolving according to

$$\frac{\partial\omega(V,t)}{\partial t} = -\frac{\partial F(V)\omega(V,t)}{\partial V} + \frac{B}{2}\frac{\partial^2\omega(V,t)}{\partial V^2} \tag{D6}$$

and by performing integration in time we get

$$-VW_{\rm st}(V) = -\frac{d}{dV}F(V)\rho(V) + \frac{B}{2}\frac{d^2\rho(V)}{dV^2}. \tag{D7}$$

Integrating this equation, with boundary conditions $W_{\rm st}(V\to\pm\infty) = 0$, we get

$$\rho(V) = W_{\rm st}(V)\int_{-\infty}^V dV'\frac{2f(V')}{BW_{\rm st}(V')} \tag{D8}$$

with

$$f(V) = -\int_{-\infty}^{V} dV' V' W_{\rm st}(V'). \tag{D9}$$

Inserting the result for ρ in Eq. (D5) and performing integration by parts, we finally get

$$D_{\rm eff} = \int_{-\infty}^{\infty} dV \frac{2f(V)^2}{B W_{\rm st}(V)}. \tag{D10}$$

Applying this result to our problem, we get $W_{\rm st}$ given by

$$W_{\rm st} = \frac{e^{-(3\gamma^2/2B)T^3}}{\sqrt{3\gamma T^3} K_{1/4}\left(\frac{3\gamma^2}{2B}T^3\right)} e^{-(\gamma V^2 + V^4/12T^3)/B}, \tag{D11}$$

where $K_n(x)$ is the modified Bessel function of the second kind. After calculating $f(V)$ the integral in Eq. (D10) becomes

$$D_{\rm eff} = \frac{\pi}{2}\sqrt{\frac{3T^3}{\gamma}} \frac{e^{-(9\gamma^2/2B)T^3}}{K_{1/4}\left(\frac{3\gamma^2}{2B}T^3\right)} \int_{-\infty}^{\infty} dV \times \operatorname{erfc}\left(\frac{6\gamma T^3 + V^2}{\sqrt{12BT^3}}\right)^2 e^{(\gamma V^2 + V^4/12T^3)/B}, \tag{D12}$$

where erfc is the complementary error function, $\operatorname{erfc} = 1 - \operatorname{erf}$. The integral in Eq. (D12) can be calculated for $T = T_c$, where $\gamma = 0$, to be

$$D_{\rm eff} = \frac{3\Gamma\left(\frac{1}{4}\right)}{16(5184)^{1/4}\Gamma\left(\frac{5}{4}\right)}\left[3\pi - \sqrt{2}\,{}_3F_2\left(\frac{3}{4},1,\frac{5}{4};\frac{3}{2},\frac{7}{4};1\right)\right] = 0.365\,622\ldots, \tag{D13}$$

where $\Gamma(x)$ is the Euler Gamma function and ${}_pF_q$ is the generalized hypergeometric function.

APPENDIX E: CALCULATION OF DIFFUSION COEFFICIENT FOR $T < T^*$

Here we calculate the spatial diffusion coefficient for the imbalanced case. Consider a particle with two possible velocities V_1 and $-V_2$. The transition rate from $-V_2$ to V_1 is α_1 and the transition rate from V_1 to $-V_2$ is α_2. We now estimate the velocity autocorrelation to estimate $D_{\rm eff}$ from Eq. (D3). We begin by writing the master equations

$$\frac{dP(V_1,t)}{dt} = \alpha_1 P(-V_2,t) - \alpha_2 P(V_1,t),$$
$$\frac{dP(V_2,t)}{dt} = \alpha_2 P(V_1,t) - \alpha_1 P(-V_2,t), \tag{E1}$$

which are solved by

$$P(V_1,t) = \frac{\alpha_1}{\alpha_1+\alpha_2} - \left(\frac{\alpha_1}{\alpha_1+\alpha_2} - P(V_1,0)\right)e^{-(\alpha_1+\alpha_2)t},$$
$$P(V_2,t) = \frac{\alpha_2}{\alpha_1+\alpha_2} + \left(\frac{\alpha_1}{\alpha_1+\alpha_2} - P(V_1,0)\right)e^{-(\alpha_1+\alpha_2)t}. \tag{E2}$$

The autocorrelation in the long time limit is then

$$\langle V(0)V(t)\rangle = \langle V(0)V(t)|V(0) = V_1\rangle \frac{\alpha_1}{\alpha_1+\alpha_2} + \langle V(0)V(t)|V(0) = -V_2\rangle \frac{\alpha_2}{\alpha_1+\alpha_2}. \tag{E3}$$

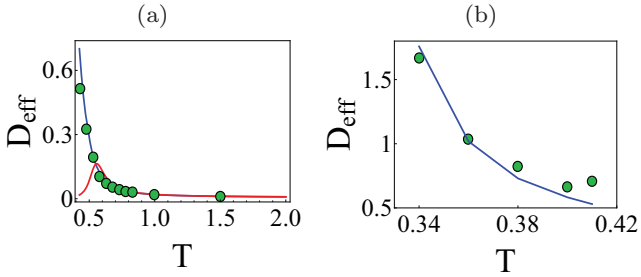

FIG. 9. Diffusion of imbalanced groups. (a) Spatial diffusion coefficient for $T > T^*$. Green points are estimated from simulation results. The blue curve is the numerical integration of Eq. (D10) [using Eqs. (F4) and (F5)] and the red line is the approximation given in Eq. (F3). (b) Spatial diffusion coefficient for $T < T^*$. Green points are estimated from simulation results. The blue curve is Eq. (E5), where α is estimated from simulations.

Calculating the conditional means, one gets

$$\langle V(0)V(t)\rangle = \frac{\alpha_1\alpha_2(V_1+V_2)^2}{(\alpha_1+\alpha_2)^3} e^{-(\alpha_1+\alpha_2)t} + \langle V\rangle^2, \tag{E4}$$

where $\langle V\rangle = \frac{\alpha_1}{\alpha_1+\alpha_2}V_1 - \frac{\alpha_2}{\alpha_1+\alpha_2}V_2$ and as we estimate $D_{\rm eff}$ in the moving frame we use $\langle V(0)V(t)\rangle - \langle V\rangle^2$ in Eq. (D3). This yields

$$D_{\rm eff} = \frac{\alpha_1(T)\alpha_2(T)(V_1+V_2)^2}{[\alpha_1(T)+\alpha_2(T)]^3}. \tag{E5}$$

To get the results in Figs. 3(d)–3(f) and 9 we first extract the rates from simulation results of the distribution of times that the group has positive or negative velocity.

APPENDIX F: CALCULATION OF DIFFUSION COEFFICIENT: IMBALANCED CASE

The Langevin equation of the imbalanced case (up to cubic order in V), for $T > T_c$, is

$$\frac{dV}{dt} = -\gamma(T)V - \frac{1}{6}\left(\frac{V}{T}\right)^3 + h + \sqrt{B}\eta(t). \tag{F1}$$

We linearize Eq. (F1) around $V^*(T)$ defined as the solution of Eq. (7). Switching to the new variable $u = V - V^*$ in Eq. (F1),

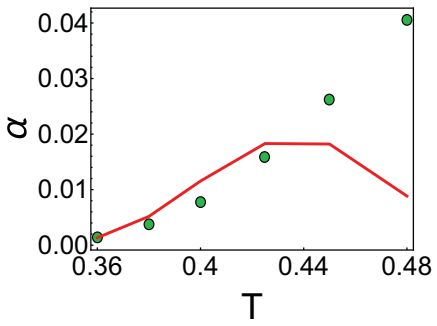

FIG. 10. Comparison between the rate of changing direction of speed (1D motion) and the Kramers escape rate (G7) for a symmetric system with $N = 50$ spins.

we get

$$\frac{du}{dt} = -\left(\gamma(T) + \frac{V^{*2}(T)}{2T^3}\right)u + \sqrt{B}\eta(t) \tag{F2}$$

up to linear order in u and the diffusion coefficient is

$$D_{\text{eff}} = \frac{B}{2\left(\gamma(T) + \frac{V^{*2}(T)}{2T^3}\right)^2}. \tag{F3}$$

We see in Fig. 9(a) that Eq. (F3) is a good approximation down to $T \simeq 0.6$.

In order to obtain a description for lower temperatures, we resort to a numerical calculation of D_{eff} by using Eq. (D10), where W_{st} is the solution of the Fokker-Planck equation including the $\tanh(V)$ term

$$W_{\text{st}} = \frac{\exp\left\{-\frac{2}{B}\left[\frac{V^2}{2} - \frac{T}{2}\log\cosh\left(\frac{V}{T}\right) - hV\right]\right\}}{\int_{-1/2+h}^{1/2+h} dV' \exp\left\{-\frac{2}{B}\left[\frac{V'^2}{2} - \frac{T}{2}\log\cosh\left(\frac{V'}{T}\right) - hV'\right]\right\}} \tag{F4}$$

and

$$f(V) = \int_{-1/2+h}^{V} dV'(V' - \langle V'\rangle)W_{\text{st}}(V'). \tag{F5}$$

The domain of the probability distribution in Eqs. (F4) and (F5) is $[-1/2+h, 1/2+h]$ as the velocity cannot have values outside this interval. We compare it with the data obtained from simulation in Fig. 9(b) to find good agreement:

$$T^* = T_c - \left(\frac{3h}{2\sqrt{2}}\right)^{2/3}. \tag{F6}$$

For $T < T^*$ the walk is ballistic on short time scales, while on long time scales it is a imbalanced random walk due to the jumps between the stable and metastable speeds.

APPENDIX G: KRAMERS ESCAPE FORMULA

The probability density of V evolves according the Fokker-Planck equation

$$\frac{\partial W}{\partial t} = \frac{\partial}{\partial V}\left[V - \frac{1}{2}\tanh\left(\frac{V}{T}\right)\right]W + \frac{B}{2}\frac{\partial^2 W}{\partial V^2}. \tag{G1}$$

We consider a quasistationary scenario $\partial W/\partial t \approx 0$. In this case we can integrate Eq. (G1) to get the approximate current

$$J = \frac{Be^{(2/B)\mathcal{G}(V_{\min})}W(V_{\min},t)}{\int_{V_{\min}}^{A} dV e^{(2/B)\mathcal{G}(V)}}, \tag{G2}$$

where $\mathcal{G}$ is the free energy of the Ising model,

$$\mathcal{G}(V) = \frac{V^2}{2} - \frac{T}{2}\log\cosh\left(\frac{V}{T}\right), \tag{G3}$$

$B = B(V_{\min})$ is the velocity diffusion coefficient calculated from Eq. (5) for $V = V_{\min}$, $V_{\min}$ is the location of the free-energy minimum, and A is a point beyond the barrier such that the particle escaped from the minimum. On the other hand, the quasistationary probability of being around the minimum is given by

$$p = W(V_{\min},t)e^{(2/B)\mathcal{G}(V_{\min})}\int_{V_1}^{V_2} dV e^{-(2/B)\mathcal{G}(V)}, \tag{G4}$$

where V_1 and V_2 are points near $V_{\min}$. We note that $J = pr$, where r is the escape rate from the minimum. Therefore, we get, from Eqs. (G2) and (G4),

$$r = \frac{J}{p} = \frac{B}{2\int_{V_{\min}}^{A} dV e^{(2/B)\mathcal{G}(V)}\int_{V_1}^{V_2} dV e^{-(2/B)\mathcal{G}(V)}}. \tag{G5}$$

Finally, we note that the integrals in Eq. (G5) have the most contribution from either $V_{\min}$ or $V_{\max}$ (the location of the barrier). Therefore, we use the following approximations:

$$\begin{aligned}\mathcal{G}(V) &\approx \mathcal{G}(V_{\min}) + \mathcal{G}''(V_{\min})(V - V_{\min})^2,\\ \mathcal{G}(V) &\approx \mathcal{G}(V_{\max}) + \mathcal{G}''(V_{\max})(V - V_{\max})^2.\end{aligned} \tag{G6}$$

Performing these Gaussian integrals from $-\infty$ to $+\infty$ leads us to the Kramers escape rate [24]

$$\begin{aligned}r = &\frac{1}{2\pi}\sqrt{\mathcal{G}''(V_{\min})|\mathcal{G}''(V_{\max})|}\\ &\times \exp\left[-\left(\frac{\mathcal{G}(V_{\max}) - \mathcal{G}(V_{\min})}{B(V_{\min})}\right)\right]\end{aligned} \tag{G7}$$

and $V_{\max}$ is the maximum (or the barrier) of the energy the particle needs to cross (in our case, $V_{\max} = 0$). We compare Eq. (G7) with simulation results for the balanced scenario in Fig. 10. We see that the Kramers formula agrees with the data for $T \lesssim 0.38$.

APPENDIX H: MINORITY PROBABILITY IN THE LIMIT $T \to 0$

Our initial conditions are such that each spin is active with probability $1/2$. Therefore, the initial V is negative with probability P_-, zero with probability P_0, and positive with probability P_+. In the limit $T \to 0$ the target that is reached is determined by the sign of the initial V. We get

$$P_{\min} = P_- + \tfrac{24}{50}P_0. \tag{H1}$$

We can see the initial condition of each side as a random walk. A spin $+1$ corresponds to a positive step of the walk and a spin -1 corresponds to a step in the negative direction. Since one side has 26 steps and the other 24 steps we have a walker with 26 steps and the other with 24 steps. Within this framework, $P_{-(+)}$ is the probability that the 24 (26) walker is at the greatest position while P_0 is the probability that the two walkers are at the same position. We first consider a case where the two walkers make N_2 steps (24 in this example) and then the majority (N_1) walker gets a bonus of $N_1 - N_2$ (i.e., two in our example) steps. The difference between the two walkers after n steps, Y_n, is given by a random walk with pauses. Notice that if the difference of the two walkers is Y_n, then there is a difference of $Y_n/2$ positive spins between the two sides. The probability of the difference is a sum over trinomial distributions

$$P(Y_n = 2k) = \frac{1}{2^n}\sum_{m=0}^{n/2}\frac{n!}{(n-2m)!(m-k)!(m+k)!}\left(\frac{1}{2}\right)^{2m}. \tag{H2}$$

We find the following exact results:

$$P(Y_n=0)=\frac{\left(n-\frac{1}{2}\right)!}{\sqrt{\pi}n!},$$
$$P(Y_n=\pm 2)=\frac{n(n-1)\left(n-\frac{1}{2}\right)!}{\sqrt{\pi}(n+2)!}. \quad \text{(H3)}$$

For bigger differences we can get numerical estimates. Note that $Y_n=-2$ implies that there is one more positive spin in the minority direction (before we counted the two extra spins). In this case the only way to get a minority-dominated side (corresponding to P_-) is that the extra two spins in the majority side are negative. This occurs with Prob $=1/4$. Taking all the combinations into account, we get

$$P_-=P(Y_{24}=-2)\tfrac{1}{4}+P(Y_{24}=-4)\tfrac{3}{4}+P(Y_{24}<-4),$$
$$P_+=P(Y_{24}=-2)\tfrac{1}{4}+P(Y_{24}=0)\tfrac{3}{4}+P(Y_{24}>0),$$
$$P_0=1-P_--P_+. \quad \text{(H4)}$$

Returning to Eq. (H1) and substituting numbers, we get

$$P_{\min}=0.399\,11. \quad \text{(H5)}$$

APPENDIX I: ORDER PARAMETER CALCULATION FOR A GROUP MOVING IN TWO DIMENSIONS

We wish to characterize the group moving in two dimensions with the Hamiltonian (14). The equilibrium behavior can be derived from the partition function, which is (assuming $N\gg 1$)

$$Z=\mathrm{Tr}_\sigma \exp\left[\frac{1}{NT}\left(\sum_i \hat{p}_i\sigma_i\right)^2\right]. \quad \text{(I1)}$$

By introducing the auxiliary fields $\vec{V}_{\rm tot}$ and using the identity $\int_{-\infty}^{\infty}dx\,dy\,e^{-a(x^2+y^2)+bx+cy}=(\pi/a)e^{(b^2+c^2)/4a}$, we get

$$Z\sim \mathrm{Tr}_\sigma\int dV_x dV_y \exp\left(-\frac{N}{T}(\vec{V}_{\rm tot})^2+2\frac{\vec{V}_{\rm tot}\cdot\sum_i \hat{p}_i\sigma_i}{T}\right), \quad \text{(I2)}$$

with $a=N/T$. After summing over σ_i and a bit of algebra the partition takes the form

$$Z\sim\int dV_x dV_y e^{-(N/T)\mathcal{G}(\vec{V}_{\rm tot},T)}, \quad \text{(I3)}$$

with

$$\mathcal{G}=(\vec{V}_{\rm tot})^2-\frac{T}{2}\left[\log\left(1+e^{2\frac{\vec{V}_{\rm tot}\cdot\hat{p}_1}{T}}\right)+\log\left(1+e^{2\frac{\vec{V}_{\rm tot}\cdot\hat{p}_2}{T}}\right)\right]. \quad \text{(I4)}$$

In the limit $N\gg 1$ the integral in Eq. (I3) is dominated by $\vec{V}^*_{\rm tot}=\arg\min_{V_{\rm tot}}\mathcal{G}(\vec{V}_{\rm tot},T)$. Thus we can get the mean velocity components in the system by solving the equations $\frac{\partial\mathcal{G}}{\partial V_x}=0$ and $\frac{\partial\mathcal{G}}{\partial V_y}=0$. By the form of the resulting equations we see that the auxiliary field is $\vec{V}_{\rm tot}=\frac{1}{N}\sum\hat{p}_i\langle\sigma_i\rangle$.

Writing $(V_x,V_y)=(f_x\cos(\frac{\theta}{2}),f_y\sin(\frac{\theta}{2}))$ and solving the equation for f_x up to second order in f_y, we find

$$f_x=f_{x0}+\frac{2}{T}\frac{\sin\left(\frac{\theta}{2}\right)^4\tanh\left(\frac{f_{x0}\cos(\frac{\theta}{2})}{T}\right)}{1-2T+\cos(\theta)-2T\cosh\left(2f_{x0}\frac{\cos(\frac{\theta}{2})}{T}\right)}(f_y)^2,$$
$$f_{x0}=\frac{1}{1+e^{-2f_{x0}\cos(\theta/2)^2/T}}. \quad \text{(I5)}$$

Inserting these results into the equation $V_y:\frac{\partial\mathcal{G}}{\partial V_y}=0$, we can think of it as derived from an effective free energy $\mathcal{G}_{\rm eff}=\frac{a}{2}(f_y)^2+\frac{b}{4}(f_y)^4$ with

$$a=\frac{2\exp\left(-2\frac{f_{x0}\cos(\frac{\theta}{2})^2}{T}\right)\sin\left(\frac{\theta}{2}\right)^2}{T\left[1+\exp\left(-2\frac{f_{x0}\cos(\frac{\theta}{2})^2}{T}\right)\right]^2}-1, \quad \text{(I6)}$$

$$b=\frac{\sin\left(\frac{\theta}{2}\right)^6}{\cosh\left(\frac{f_{x0}\cos(\frac{\theta}{2})^2}{T}\right)^4}\frac{1+3T+\cos(\theta)-2[1-T+\cos(\theta)]\cosh\left(2\frac{f_{x0}\cos(\frac{\theta}{2})}{T}\right)-T\cosh\left(4\frac{f_{x0}\cos(\frac{\theta}{2})}{T}\right)}{6T^3\left[2T-1-\cos(\theta)+2T\cosh\left(2\frac{f_{x0}\cos(\frac{\theta}{2})}{T}\right)\right]}. \quad \text{(I7)}$$

The model exhibits both second- and first-order transitions. The transition changes its nature at the tricritical point where $a=0$ and $b=0$. Solving it we get $T_3=0.318\,747$ and $\theta_3=2.191\,53$.

APPENDIX J: ASYMMETRIC GROUPS

We also calculate the order parameter for subgroups of nonequal sizes. The equivalent of the free energy in Eq. (I4) is

$$\mathcal{G}=(\vec{V}_{\rm tot})^2-\frac{T}{2}[(1+\epsilon)\log(1+e^{2(\vec{V}_{\rm tot}\cdot\hat{p}_1/T)})$$
$$+(1-\epsilon)\log(1+e^{2(\vec{V}_{\rm tot}\cdot\hat{p}_2/T)})], \quad \text{(J1)}$$

where ϵ is the strength of the asymmetry between the two subgroups. We show the groups' directions in Fig. 11.

APPENDIX K: DYNAMICS OF GROUP MOVING TO A TARGET

Consider two targets located at $(x_1,y_1)=(X,Y)$ and $(x_2,y_2)=(X,-Y)$ with the group starting from $(x_g(0),y_g(0))=(0,0)$. As for the one-dimensional case, at each time step one of the spins is updated by Glauber dynamics, $r=(1+e^{\Delta H/T})^{-1}$ [using the Hamiltonian H in Eq. (14)], and the location of the group is updated

$$x_g(t+\Delta t)=x_g(t)+V_x\Delta t,$$
$$y_g(t+\Delta t)=y_g(t)+V_y\Delta t. \quad \text{(K1)}$$

We take the convention that in a single time unit, on average, all the particle are updated. Therefore, each update is defined as $\Delta t=1/N$.

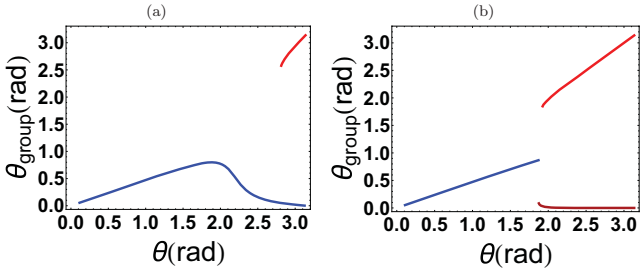

FIG. 11. Group direction with unequal subgroups [$\epsilon = -0.1$ in Eq. (J1)] for (a) $T = 0.4$ and (b) $T = 0.1$. The darker red curve is the minimum of the free energy (the lighter red curve is the metastable solution).

APPENDIX L: SECOND SPIN MODEL

In this model the informed individuals in each subgroup do not switch between applying a social force or not, as in the spin model explained in the main text, but rather they are always applying a social force. However, they can switch between applying this social force in their own preferred direction or in the direction of the competing subgroup. In this model the spin variable describes the direction along which the force is applied. Each spin feels, in addition to the total applied force, also an internal magnetic field that gives it a bias to point in its preferred direction.

The new model Hamiltonian is

$$H = -\frac{J}{N}\sum_{i\neq j}\hat{p}_i\hat{p}_j - \hat{h}_1\sum_{i\in 1}\hat{p}_i - \hat{h}_2\sum_{i\in 2}\hat{p}_i, \tag{L1}$$

where $\hat{p}_i = \cos(\theta/2)\hat{x} \pm \sin(\theta/2)\hat{y}$ are the spin degrees of freedom and $\hat{h}_{1\,(2)} = h[\cos(\theta/2)\hat{x} + (-)\sin(\theta/2)\hat{y}]$ are the magnetic fields that denote the two preferred directions, which are constant. The Hamiltonian describes a ferromagnetic interaction of each spin with the average field of the other spins in addition to its internal bias. The Hamiltonian can be rewritten in terms of variables $s_i = \pm 1$ as $\hat{p}_i = \cos(\theta/2)\hat{x} + s_i\sin(\theta/2)\hat{y}$. The Hamiltonian takes the form

$$H = -\frac{J}{N}\sin\left(\frac{\theta}{2}\right)^2\sum_{i\neq j}s_is_j - h\sin\left(\frac{\theta}{2}\right)^2\sum_{i\in 1}s_i + h\sin\left(\frac{\theta}{2}\right)^2\sum_{i\in 2}s_i. \tag{L2}$$

We see in Eq. (L2) that the angular conflict θ can be factored out of the entire Hamiltonian, which is not the case for the Hamiltonian in the main model (14). Standard mean-field procedure leads to the means of the two subgroups

$$\langle s\rangle_1 = \tanh\left[\frac{2Jm+h}{T}\sin\left(\frac{\theta}{2}\right)^2\right],$$
$$\langle s\rangle_2 = \tanh\left[\frac{2Jm-h}{T}\sin\left(\frac{\theta}{2}\right)^2\right], \tag{L3}$$

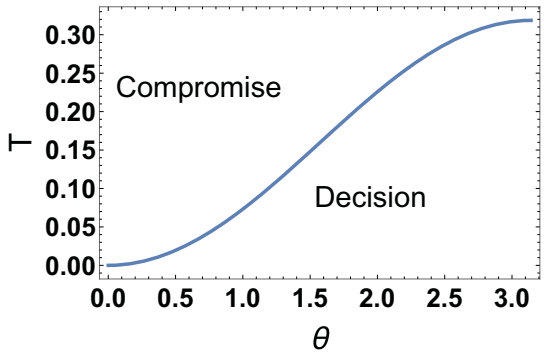

FIG. 12. Phase diagram for the second spin model, showing the transition line between the compromise and decision regimes according to Eq. (L5).

where $m = \sum s_i/N$ is the average magnetization. The self-consistent equation for the order parameter is then

$$m = \frac{\tanh\left(\frac{2Jm+h}{T}\sin\left(\frac{\theta}{2}\right)^2\right) + \tanh\left(\frac{2Jm-h}{T}\sin\left(\frac{\theta}{2}\right)^2\right)}{2}. \tag{L4}$$

By defining $T' = T/\sin(\frac{\theta}{2})^2$ we get a model that is independent of the angular difference. Therefore, for the critical temperature we write

$$T_c(\theta) = T_c(\pi)\sin\left(\frac{\theta}{2}\right)^2, \tag{L5}$$

which suggest that a transition is possible for every finite angular difference (Fig. 12), with the critical angle vanishing in the limit of $T \to 0$ (or $N_{ui} \to \infty$), which does not seem to agree with the results of the flock model [Fig. 1(e)].

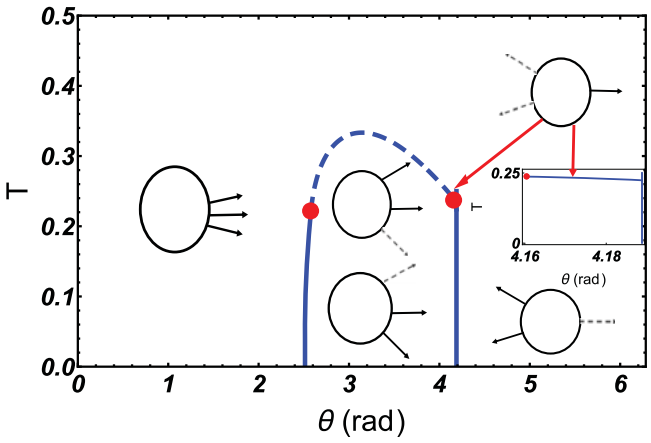

FIG. 13. Phase diagram for a decision between three directions. The dashed curve is the second-order transition while the solid curve is the first-order curve. Red points are tricritical points. Within each region the configuration of the free-energy minimum is shown. The inset shows a close-up of the region next to the second tricritical point.

APPENDIX M: DECISION-MAKING BETWEEN THREE PREFERRED DIRECTIONS

In this case the directions are defined as

$$\hat{p}_0 = \hat{x}, \quad \hat{p}_1 = \cos\left(\frac{\theta}{2}\right)\hat{x} + \sin\left(\frac{\theta}{2}\right)\hat{y}, \tag{M1}$$

$$\hat{p}_2 = \cos\left(\frac{\theta}{2}\right)\hat{x} - \sin\left(\frac{\theta}{2}\right)\hat{y} \tag{M2}$$

and the Hamiltonian has the same form as in Eq. (14). An analysis similar to the one in the two-direction case leads to the following free energy:

$$\mathcal{G} = (\vec{V}_{\rm tot})^2 - \frac{T}{3}[\log(1 + e^{2(V_x/T)}) + \log(1 + e^{2(\vec{V}_{\rm tot}\cdot\hat{p}_1 T)}) + \log(1 + e^{2(\vec{V}_{\rm tot}\cdot\hat{p}_2/T)})]. \tag{M3}$$

Analyzing this system, we find two tricritical points. The structure of the free-energy landscape is such that complete decision is never the minimum of the landscape. The transition is between a compromise of all three directions to a compromise of two directions. As the angular difference is increasing, the compromise state changes to be formed from the two backward directions. We show the phase diagram and the free-energy minimum configurations in Fig. 13.

[1] T. Vicsek and A. Zafeiris, Phys. Rep. **517**, 71 (2012).
[2] C. C. Ioannou, V. Guttal, and I. D. Couzin, Science **337**, 1212 (2012).
[3] A. Berdahl, C. J. Torney, C. C. Ioannou, J. J. Faria, and I. D. Couzin, Science **339**, 574 (2013).
[4] A. J. Ward, D. J. Sumpter, I. D. Couzin, P. J. Hart, and J. Krause, Proc. Natl. Acad. Sci. U.S.A. **105**, 6948 (2008).
[5] D. J. Sumpter, J. Krause, R. James, I. D. Couzin, and A. J. Ward, Curr. Biol. **18**, 1773 (2008).
[6] A. Strandburg-Peshkin, D. R. Farine, I. D. Couzin, and M. C. Crofoot, Science **348**, 1358 (2015).
[7] S. B. Rosenthal, C. R. Twomey, A. T. Hartnett, H. S. Wu, and I. D. Couzin, Proc. Natl. Acad. Sci. U.S.A. **112**, 4690 (2015).
[8] I. D. Couzin, J. Krause, N. R. Franks, and S. A. Levin, Nature (London) **433**, 513 (2005).
[9] D. Biro, D. J. Sumpter, J. Meade, and T. Guilford, Curr. Biol. **16**, 2123 (2006).
[10] N. E. Leonard, T. Shen, B. Nabet, L. Scardovi, I. D. Couzin, and S. A. Levin, Proc. Natl. Acad. Sci. U.S.A. **109**, 227 (2012).
[11] A. T. Hartnett, E. Schertzer, S. A. Levin, and I. D. Couzin, Phys. Rev. Lett. **116**, 038701 (2016).
[12] L. Conradt and T. J. Roper, Nature (London) **421**, 155 (2003).
[13] L. Feigenson, S. Dehaene, and E. Spelke, Trends Cognit. Sci. **8**, 307 (2004).
[14] S. Arganda, A. Pérez-Escudero, and G. G. de Polavieja, Proc. Natl. Acad. Sci. U.S.A. **109**, 20508 (2012).
[15] I. D. Couzin, C. C. Ioannou, G. Demirel, T. Gross, C. J. Torney, A. Hartnett, L. Conradt, S. A. Levin, and N. E. Leonard, Science **334**, 1578 (2011).
[16] M. Marchetti, J. Joanny, S. Ramaswamy, T. Liverpool, J. Prost, M. Rao, and R. A. Simha, Rev. Mod. Phys. **85**, 1143 (2013).
[17] T. Vicsek, A. Czirók, E. Ben-Jacob, I. Cohen, and O. Shochet, Phys. Rev. Lett. **75**, 1226 (1995).
[18] M. Nagy, I. Daruka, and T. Vicsek, Physica A **373**, 445 (2007).
[19] S. Galam, Y. Gefen, and Y. Shapir, J. Math. Soc. **9**, 1 (1982).
[20] A. Gelblum, I. Pinkoviezky, E. Fonio, A. Ghosh, N. Gov, and O. Feinerman, Nat. Commun. **6**, 7729 (2015).
[21] M. Kac, G. Uhlenbeck, and P. Hemmer, J. Math. Phys. **4**, 216 (1963).
[22] R. K. Pathria and P. D. Beale, *Statistical Mechanics*, 3rd ed. (Academic, New York, 2011).
[23] R. Kubo, Rep. Prog. Phys. **29**, 255 (1966).
[24] H. Risken, *The Fokker-Planck Equation*, Springer Series in Synergetics Vol. 18 (Springer, Berlin, 1984).
[25] A. Einstein, Ann. Phys. (Leipzig) **17**, 549 (1905).
[26] B. Lindner, New J. Phys. **9**, 136 (2007).
[27] S. Redner, *A Guide to First-Passage Processes* (Cambridge University Press, Cambridge, 2001).
[28] N. Miller, S. Garnier, A. T. Hartnett, and I. D. Couzin, Proc. Natl. Acad. Sci. U.S.A. **110**, 5263 (2013).
[29] S. Galam and S. Moscovici, Eur. J. Soc. Psych. **21**, 49 (1991).
[30] S. Galam, Physica A **238**, 66 (1997).
[31] G. Sella and A. E. Hirsh, Proc. Natl. Acad. Sci. U.S.A. **102**, 9541 (2005).
[32] C. K. Fisher and P. Mehta, Proc. Natl. Acad. Sci. U.S.A. **111**, 13111 (2014).
[33] R. Bogacz, Trends Cognit. Sci. **11**, 118 (2007).
[34] R. J. Glauber, J. Math. Phys. **4**, 294 (1963).
[35] P. L. Krapivsky, S. Redner, and E. Ben-Naim, *A Kinetic View of Statistical Physics* (Cambridge University Press, Cambridge, 2010).